Turbulent diffusion of chemically reacting flows: Theory and numerical simulations

T. Elperin,[1,*] N. Kleeorin,[1,†] M. Liberman,[2,‡] A. N. Lipatnikov,[3,§] I. Rogachevskii,[1,‖] and R. Yu[4,¶]

[1]*The Pearlstone Center for Aeronautical Engineering Studies, Department of Mechanical Engineering, Ben-Gurion University of the Negev, P.O. Box 653, Beer-Sheva 84105, Israel*

[2]*Nordita, KTH Royal Institute of Technology and Stockholm University, Roslagstullsbacken 23, 10691 Stockholm, Sweden*

[3]*Department of Applied Mechanics, Chalmers University of Technology, Göteborg 412 96, Sweden*

[4]*Division of Fluid Mechanics, Lund University, Lund 221 00, Sweden*

(Received 8 December 2016; revised manuscript received 19 August 2017; published 22 November 2017)

The theory of turbulent diffusion of chemically reacting gaseous admixtures developed previously [T. Elperin *et al.*, Phys. Rev. E **90**, 053001 (2014)] is generalized for large yet finite Reynolds numbers and the dependence of turbulent diffusion coefficient on two parameters, the Reynolds number and Damköhler number (which characterizes a ratio of turbulent and reaction time scales), is obtained. Three-dimensional direct numerical simulations (DNSs) of a finite-thickness reaction wave for the first-order chemical reactions propagating in forced, homogeneous, isotropic, and incompressible turbulence are performed to validate the theoretically predicted effect of chemical reactions on turbulent diffusion. It is shown that the obtained DNS results are in good agreement with the developed theory.

DOI: 10.1103/PhysRevE.96.053111

I. INTRODUCTION

Effect of chemical reactions on turbulent transport is of great importance in many applications ranging from atmospheric turbulence and transport of pollutants to combustion processes (see, e.g., [1–8]). For instance, significant influence of combustion on turbulent transport is well known [8–13] to cause the so-called countergradient scalar transport, i.e., a flux of products from unburned to burned regions of a premixed flame. In turn, the countergradient transport can substantially reduce the flame speed [14–16] and therefore is of great importance for calculations of burning rate and plays a key role in the premixed turbulent combustion.

It is worth remembering, however, that the countergradient transport appears to be an indirect manifestation of the influence of chemical reactions on turbulent fluxes, as this manifestation is controlled by density variations due to heat release in combustion reactions rather than by the reactions themselves. As far as the straightforward influence of reactions on turbulent transport [17] is concerned, such effects have been addressed in a few studies [8,18,19] of premixed flames. Because the easiest way to study such a straightforward influence consists in investigating a constant-density reacting flow, the density is considered to be constant in the present paper.

The effect of chemical reactions on turbulent diffusion of chemically reacting gaseous admixtures in a developed turbulence has been studied analytically using a path-integral approach for a δ-correlated-in-time random velocity field [20]. This phenomenon also has been recently investigated by applying the spectral-τ approach that is valid for large Reynolds and Péclet numbers [21]. These studies have demonstrated that turbulent diffusion of the reacting species can be strongly suppressed with increasing Damköhler number $\mathrm{Da} = \tau_0/\tau_c$, which is a ratio of turbulent τ_0 and chemical τ_c time scales.

The dependence of the turbulent diffusion coefficient D_T on the turbulent Damköhler number obtained theoretically in [21] was validated using the results of mean-field simulations (MFSs) of a reactive front propagating in a turbulent flow [22]. In these simulations, the mean speed s_T of the planar one-dimensional reactive front was determined using numerical solution of the Kolmogorov-Petrovskii-Piskunov (KPP) equation [23] or the Fisher equation [24]. This mean-field equation was extended in [22] to take into account memory effects of turbulent diffusion when the turbulent time was much larger than the characteristic chemical time. Turbulent diffusion coefficients as a function of Da were determined numerically in [22] using the obtained function $s_T(\mathrm{Da})$ and invoking the well-known expression $s_T = 2(D_T/\tau_c)^{1/2}$. The theoretical dependence $D_T(\mathrm{Da})$ derived in [21] was in good agreement with the numerical results of MFSs [22].

In the present study we have generalized the theory [21] of turbulent diffusion in reacting flows for finite Reynolds numbers and have obtained the dependence of the turbulent diffusion coefficient on two parameters: the Reynolds number and the Damköhler number. The generalized theory has been validated by comparing its predictions with the three-dimensional direct numerical simulations (DNSs) of the reaction wave propagating in a homogeneous isotropic and incompressible turbulence for a wide range of ratios of the wave speed to the rms turbulent velocity and different Reynolds numbers.

It is worth stressing that the previous validation of the original theory by MFS [21] and present validation of the generalized theory by DNS complement each other, because they were performed using different methods. Indeed, the previous validation [21] was performed by evaluating D_T using numerical data [22] on the mean reaction front speed obtained by solving a statistically planar one-dimensional mean KPP equation, with such a MFS method implying spatial

*elperin@bgu.ac.il; http://www.bgu.ac.il/me/staff/tov
†nat@bgu.ac.il
‡misha.liberman@gmail.com
§andrei.lipatnikov@chalmers.se
‖gary@bgu.ac.il; http://www.bgu.ac.il/∼gary
¶rixin.yu@energy.lth.se

uniformity of the turbulent diffusion coefficient. In contrast, in the present work, D_T is straightforwardly extracted from DNS data obtained by numerically integrating unsteady three-dimensional Navier-Stokes and reaction-diffusion equations, with eventual spatial variations in the turbulent diffusion coefficient being addressed.

This paper is organized as follows. The generalized theory is described in Sec. II. Direct numerical simulations performed to validate the theory are described in Sec. III. Validation results are discussed in Sec. IV. A summary is given in Sec. V.

II. EFFECT OF CHEMISTRY ON TURBULENT DIFFUSION

The goal of this section is to generalize the theory [21] by considering turbulent flows characterized by large but finite Reynolds numbers. It is worth stressing that neither the original theory [21] nor its generalization has specially been developed to study combustion. On the contrary, while the theory addresses a wide class of turbulent reacting flows, certain assumptions of the theory do not hold in premixed flames. Nevertheless, as will be shown in subsequent sections, the theoretical predictions are valid under a wider range of conditions than originally assumed and in particular under conditions associated with the straightforward influence of chemical reactions on turbulence in flames.

A. Governing equations

The equation for the scalar field in the incompressible chemically reacting turbulent flow reads

$$\frac{\partial c}{\partial t} + (\boldsymbol{v}\cdot\nabla)c = W(c) + D\Delta c, \tag{1}$$

where $c(t,\boldsymbol{x})$ is a scalar field, $\boldsymbol{v}(t,\boldsymbol{x})$ is the instantaneous fluid velocity field, D is a constant diffusion coefficient based on molecular Fick's law, and $W(c)$ is the source (or sink) term. The function $W(c)$ is usually chosen according to the Arrhenius law (to be given in the next section). We consider a simplified model of a single-step reaction typically used in numerical simulations of turbulent combustion.

The velocity $\boldsymbol{v}$ of the fluid is determined by the Navier-Stokes equation

$$\frac{\partial \boldsymbol{v}}{\partial t} + (\boldsymbol{v}\cdot\nabla)\boldsymbol{v} = -\frac{1}{\rho}\nabla p + \nu\Delta\boldsymbol{v} + \boldsymbol{f}, \tag{2}$$

where $\boldsymbol{f}$ is the external force to support turbulence, ν is the kinematic viscosity, and p and ρ are the fluid pressure and density, respectively. For an incompressible flow the fluid density is constant.

B. Procedure of derivations of turbulent flux

To determine turbulent transport coefficients, Eq. (1) is averaged over an ensemble of turbulent velocity fields. In the framework of a mean-field approach, the scalar field c is decomposed into the mean field $\langle c\rangle$ and fluctuations c', where $\langle c'\rangle = 0$ and angular brackets designate ensemble averaging. This can be considered, for example, as the averaging over an ensemble of independent snapshots taken, e.g., in numerical simulations with a time interval that is larger than the turbulent correlation time. This is similar to a sliding (window) averaging, where the sliding time is larger than the turbulent time. In this study (see the next section with the DNS results) we also employ a spatial averaging over a plane perpendicular to the direction of the front propagation, etc. The velocity field is decomposed in a similar fashion, $\boldsymbol{v} = \langle\boldsymbol{U}\rangle + \boldsymbol{u}$, assuming, for simplicity, a vanishing mean fluid velocity $\langle\boldsymbol{U}\rangle = 0$, where $\boldsymbol{u}$ are the fluid velocity fluctuations.

Using the equation for fluctuations $c' = c - \langle c\rangle$ of the scalar field and the Navier-Stokes equation for fluctuations $\boldsymbol{u}$ of the velocity field written in $\boldsymbol{k}$ space we derive an equation for the second-order moment $\langle c'\boldsymbol{u}\rangle_{\boldsymbol{k}} \equiv \langle c'(\boldsymbol{k})u_i(-\boldsymbol{k})\rangle$:

$$\frac{\partial\langle c'u_i\rangle_{\boldsymbol{k}}}{\partial t} = -\left[\tau_c^{-1} + (\nu + D)k^2\right]\langle c'u_i\rangle_{\boldsymbol{k}} + \hat{\mathcal{N}}\langle c'u_i\rangle - \langle u_i u_j\rangle_{\boldsymbol{k}}\nabla_j\langle c\rangle, \tag{3}$$

where $\langle u_i u_j\rangle_{\boldsymbol{k}} \equiv \langle u_i(\boldsymbol{k})u_j(-\boldsymbol{k})\rangle$, $\tau_c = \langle c\rangle/\langle W\rangle$ is the chemical time, $\langle W\rangle$ is the mean source function, and $\hat{\mathcal{N}}\langle c'u_i\rangle$ includes the third-order moments caused by the nonlinear terms:

$$\hat{\mathcal{N}}\langle c'u_i\rangle = -\langle[\nabla\cdot(c'\boldsymbol{u})]u_i\rangle_{\boldsymbol{k}} - \langle c'[(\boldsymbol{u}\cdot\nabla)u_i]\rangle_{\boldsymbol{k}} - \langle c'[\rho^{-1}\nabla_i p']\rangle_{\boldsymbol{k}}. \tag{4}$$

Here we follow the procedure of the derivation of the turbulent fluxes that is described in detail in [21], taking into account large yet finite Reynolds number. In particular, we use a multiscale approach (i.e., we separate fast and slow variables, where fast small-scale variables correspond to fluctuations and slow large-scale variables correspond to mean fields). Since the ratio of the spatial density of species is assumed to be much smaller than the density of the surrounding fluid (i.e., small mass-loading parameter), there is only one-way coupling, i.e., no effect of species on the fluid flow. For the same reason the energy release (or absorbtion of energy) caused by chemical reactions is much smaller than the internal energy of the surrounding fluid. This implies that even a small chemical time does not affect the fluid characteristics. Finally, we also assume that the deviations of the source term W from its mean value $\langle W\rangle$ are not large. While such an assumption does not hold in a typical premixed turbulent flame [8], we will see later that the theory well predicts the effect of the chemical reaction on turbulent transport even if the difference in $W(c)$ and $\langle W\rangle(\langle c\rangle)$ is significant, as commonly occurs in the case of premixed combustion.

The equation for the second-order moment (3) includes the first-order spatial differential operators applied to the third-order moments $\hat{\mathcal{N}}\langle c'u_i\rangle$. To close the system of equations it is necessary to express the third-order terms $\hat{\mathcal{N}}\langle c'u_i\rangle$ through the lower-order moments $\langle c'u_i\rangle_{\boldsymbol{k}}$ (see, e.g., [25–27]). We use the spectral-τ approximation that postulates that the deviations of the third-order moments $\hat{\mathcal{N}}\langle c'u_i\rangle$ from the contributions to these terms afforded by the background turbulence $\hat{\mathcal{N}}\langle c'u_i\rangle^{(0)}$ can be expressed through the similar deviations of the second-order moments $\langle c'u_i\rangle_{\boldsymbol{k}} - \langle c'u_i\rangle_{\boldsymbol{k}}^{(0)}$,

$$\hat{\mathcal{N}}\langle c'u_i\rangle - \hat{\mathcal{N}}\langle c'u_i\rangle^{(0)} = -\frac{1}{\tau_r(k)}\left[\langle c'u_i\rangle_{\boldsymbol{k}} - \langle c'u_i\rangle_{\boldsymbol{k}}^{(0)}\right] \tag{5}$$

(see, e.g., [25,26,28]), where $\tau_r(k)$ is the scale-dependent relaxation time, which can be identified with the correlation time $\tau(k)$ of the turbulent velocity field for large Reynolds

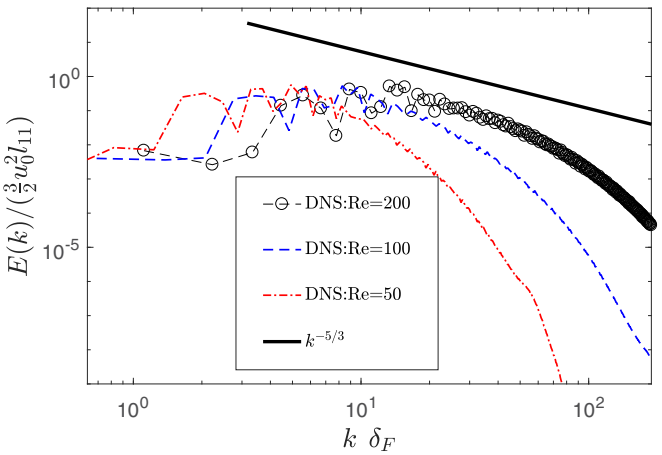

FIG. 1. Spectrum of turbulent kinetic energy.

and Péclet numbers. The functions with the superscript (0) correspond to the background turbulence with zero gradients of the mean scalar field. Validation of the τ approximation for different situations with homogeneous and inhomogeneous conditions has been performed in various numerical simulations and analytical studies (see, e.g., [29–34]). When the gradients of the mean scalar field are zero, the turbulent flux vanishes and the contributions of the corresponding fluctuations [the terms with the superscript (0)] vanish as well. Consequently, Eq. (5) reduces to $\hat{\mathcal{N}}\langle c'u_i\rangle_{\boldsymbol{k}} = -\langle c'(\boldsymbol{k})u_i(-\boldsymbol{k})\rangle/\tau(k)$.

We also assume that the characteristic times of variation of the second-order moments are substantially larger than the correlation time $\tau(k)$ for all turbulence scales. This allows us to consider the steady-state solution of Eq. (3), which yields the expression for the turbulent flux $\langle c'u_i\rangle_{\boldsymbol{k}} = \langle c'(\boldsymbol{k})u_i(-\boldsymbol{k})\rangle$ in $\boldsymbol{k}$ space,

$$\langle c'u_i\rangle_{\boldsymbol{k}} = -\tau_{\rm eff}(k)\langle u_i u_j\rangle^{(0)}_{\boldsymbol{k}}\nabla_j\langle c\rangle, \tag{6}$$

where $\tau_{\rm eff}(k) = [\tau_c^{-1} + (\nu + D)k^2 + \tau^{-1}(k)]^{-1}$ is the effective time.

We consider isotropic and inhomogeneous background turbulence $\langle u_i u_j\rangle^{(0)}_{\boldsymbol{k}} \equiv \langle u_i(\boldsymbol{k})u_j(-\boldsymbol{k})\rangle$ (see, e.g., [35]),

$$\langle u_i(\boldsymbol{k})u_j(-\boldsymbol{k})\rangle = \frac{E_T(k)}{8\pi k^2}\left[\delta_{ij} - \frac{k_i k_j}{k^2} + \frac{i}{2k^2}(k_i\nabla_j - k_j\nabla_i)\right]\langle \mathbf{u}^2\rangle, \tag{7}$$

where

$$E_T(k) = \frac{2}{3k_0}(1 - {\rm Re}^{-1/2})^{-1}\left(\frac{k}{k_0}\right)^{-5/3} \tag{8}$$

is the energy spectrum function for $k_0 \leqslant k \leqslant k_0{\rm Re}^{3/4}$, $\tau(k) = 2\tau_0(k/k_0)^{-2/3}$ is the turbulent correlation time, $k_0 = \ell_0^{-1}$, ${\rm Re} = \ell_0 u_0/\nu \gg 1$ is the Reynolds number, and $u_0 = \sqrt{\langle \mathbf{u}^2\rangle}$ is the characteristic turbulent velocity in the integral scale ℓ_0 of turbulence. The last two terms in Eq. (7) determine contributions from inhomogeneous turbulence. For comparison of the theory with DNS we do not neglect the small ${\rm Re}^{-1/2}$ term in Eq. (8).

TABLE I. DNS cases.

Case	Re	$\rm Re_\lambda$	$\eta/\Delta x$	S_L/u_0	ℓ_{11}/δ_F	$\rm Da_{DNS}$
1	50	18	0.68	0.1	2.1	0.2
2	50	18	0.68	0.2	2.1	0.4
3	50	18	0.68	0.5	2.1	1.0
4	50	18	0.68	1.0	2.1	2.1
5	50	18	0.68	2.0	2.1	4.1
6	100	30	0.86	0.1	3.7	0.4
7	100	30	0.86	0.2	3.7	0.7
8	100	30	0.86	0.5	3.7	1.9
9	100	30	0.86	1.0	3.7	3.7
10	100	30	0.86	2.0	3.7	7.5
11	200	45	1.06	0.1	6.7	0.7
12	200	45	1.06	0.2	6.7	1.3
13	200	45	1.06	0.5	6.7	3.4
14	200	45	1.06	1.0	6.7	6.7
15	200	45	1.06	2.0	6.7	13.5

C. Turbulent flux

After integration in $\boldsymbol{k}$ space we obtain the expression for the turbulent flux $\langle c'\boldsymbol{u}\rangle$,

$$\langle c'\boldsymbol{u}\rangle = \int\langle c'u_i\rangle_{\boldsymbol{k}}d\boldsymbol{k} = -D_T\nabla\langle c\rangle, \tag{9}$$

where the coefficient of turbulent diffusion D_T of the scalar field is

$$D_T = \frac{D_0^T}{\rm Da}\left[1 - \frac{\Phi({\rm Da},{\rm Re},{\rm Pr})}{1 - {\rm Re}^{-1/2}}\right], \tag{10}$$

$D_0^T = \tau_0 u_0^2/3$ is the characteristic value of the turbulent diffusion coefficient without chemical reactions, $\tau_0 = \ell_0/u_0$ is the characteristic turbulent time, the function $\Phi({\rm Da},{\rm Re},{\rm Pr})$ is

$$\Phi({\rm Da},{\rm Re},{\rm Pr}) = \int_{{\rm Re}^{-1/2}}^1 \frac{X^2 + a({\rm Re},{\rm Pr})}{2\,{\rm Da}X^3 + X^2 + a}dX, \tag{11}$$

the parameter $a({\rm Re},{\rm Pr}) = 2(1 + {\rm Pr}^{-1})/{\rm Re}$, and ${\rm Pr} = \nu/D$ is the Prandtl number. Note that the expressions for the turbulent diffusion coefficient for homogeneous and inhomogeneous turbulence are the same.

Evaluating approximately the integral in Eq. (11) by expanding the expression in the integral over a small parameter $a({\rm Re},{\rm Pr})$ for large yet finite Reynolds numbers, we obtain the following dependence of turbulent diffusion coefficient on Damköhler and Reynolds numbers:

$$D_T = \frac{D_0^T}{\rm Da}\left[1 - \frac{1}{2{\rm Da}[1 - {\rm Re}^{-1/2}]}\ln\frac{1 + 2{\rm Da}}{1 + 2{\rm Da}{\rm Re}^{-1/2}}\right] - 2D_0^T(1 + {\rm Pr}^{-1})\frac{\ln{\rm Re}}{\rm Re}. \tag{12}$$

In the limit of extremely large Reynolds numbers, we recover the result for the function $D_T({\rm Da})$ obtained in [21]:

$$D_T = \frac{D_0^T}{\rm Da}\left[1 - \frac{\ln(1 + 2\,{\rm Da})}{2\,{\rm Da}}\right]. \tag{13}$$

It follows from Eq. (12) that for small Damköhler numbers

Da $\ll 1$, the function $D_T(\mathrm{Da})$ is given by

$$D_T = D_0^T\left[1 - \frac{4\,\mathrm{Da}}{3} - 2D_0^T(1+\mathrm{Pr}^{-1})\frac{\ln \mathrm{Re}}{\mathrm{Re}} + \mathrm{Re}^{-1/2}\right], \tag{14}$$

while for large Damköhler numbers $1 \ll \mathrm{Da} \ll \mathrm{Re}^{1/2}$ it is

$$D_T = \frac{D_0^T}{\mathrm{Da}}\left[1 - \frac{\ln 2\,\mathrm{Da}}{2\,\mathrm{Da}} - 2(1+\mathrm{Pr}^{-1})\frac{\mathrm{Da}\ln \mathrm{Re}}{\mathrm{Re}}\right] \tag{15}$$

and for very large Damköhler numbers $1 \ll \mathrm{Re}^{1/2} \ll \mathrm{Da}$ it is

$$D_T = \frac{D_0^T}{\mathrm{Da}}\left[1 - 2(1+\mathrm{Pr}^{-1})\frac{\mathrm{Da}\ln \mathrm{Re}}{\mathrm{Re}}\right]. \tag{16}$$

Equations (15) and (16) show that turbulent diffusion of particles or gaseous admixtures for a large Damköhler number $\mathrm{Da} \gg 1$ is strongly reduced, i.e., $D_T = D_0^T/\mathrm{Da} = \tau_c u_0^2/3$. This implies that the turbulent diffusion for a large turbulent Damköhler number is determined by the chemical time. The underlying physics of the strong reduction of turbulent diffusion is quite transparent. For a simple first-order chemical reaction $A \to B$ the species A of the reactive admixture is consumed and its concentration decreases much faster during the chemical reaction, so the usual turbulent diffusion based on the turbulent time $\tau_0 \gg \tau_c$ does not contribute to the mass flux of a reagent A.

III. THE DNS MODEL

Direct numerical simulations of a finite-thickness reaction wave propagation in forced, homogeneous, isotropic, and incompressible turbulence for the first-order chemical reactions were performed in a fully periodic rectangular box of size of $L_x \times L_y \times L_z$ using a uniform rectangular mesh of $N_x \times N_y \times N_z$ points and a simplified in-house solver [36] developed for low-Mach-number reacting flows. Contrary to recent DNS studies by two of the present authors [37,38] that addressed self-propagation of an infinitely thin interface by solving a level set equation, the present simulations deal with a wave of a finite thickness, modeled with Eq. (1) for a single progress variable c ($c = 0$ and 1 in reactants and products, respectively), while the Navier-Stokes equation (2) was numerically integrated in both cases.

To mimic a highly nonlinear dependence of the reaction rate W on the scalar field c in a typical premixed flame characterized by significant variations in the density ρ and temperature T, the expression

$$W = \frac{1-c}{\tau_R(1+\tau)}\exp\left[-\frac{\mathrm{Ze}(1+\tau)^2}{\tau(1+c\tau)}\right] \tag{17}$$

was invoked in the present constant-density simulations. Here τ_R is a reaction time scale, while the parameters $\mathrm{Ze} = 6.0$ and $\tau = 6.0$ are counterparts of the Zeldovich number $\mathrm{Ze} = E_a(T_b - T_u)/RT_b^2$ and heat-release factor $(\rho_u - \rho_b)/\rho_b$, respectively, which are widely used in combustion theory [8–10], with subscripts u and b designating unburned and burned mixtures, respectively. Indeed, substitution of $c = (T - T_u)/(T_b - T_u)$ into the exponent in Eq. (17) results in the classical Arrhenius law

$$W = \frac{1-c}{\tau_R(1+\tau)}\exp\left(-\frac{E_a}{RT}\right), \tag{18}$$

i.e., Eq. (17) does allow us to mimic the behavior of the reaction rate in a flame by considering constant-density reacting flows. It is worth recalling that a simplification of a constant density is helpful for studying the straightforward influence of chemical reactions on turbulent transport, as already pointed out in Sec. I.

The speed S_L of the propagation of the reaction wave in the laminar flow, the wave thickness $\delta_F = D/S_L$, and the wave time scale $\tau_F = \delta_F/S_L$ were varied by changing the diffusion coefficient D and the reaction time scale τ_R, which were constant input parameters for each DNS run. The speed S_L was determined by numerically solving the one-dimensional equation (1) with $\boldsymbol{v} = 0$.

The present DNSs are similar to DNSs discussed in detail in [37,38], except for replacing a level set equations used in [37,38] by Eqs. (1) and (17). Therefore, we will restrict ourselves to a very brief summary of the simulations. A more detailed discussion of the simulations can be found in recent papers [39,40].

The boundary conditions were periodic not only in the transverse directions y and z, but also in the direction x normal to the mean wave surface. In other words, when the reaction wave reached the left boundary ($x = 0$) of the computational domain, the identical reaction wave entered the domain through its right boundary ($x = L_x$).

The initial turbulence field was generated by synthesizing prescribed Fourier waves [41] with an initial rms velocity u_0 and the forcing scale $\ell_f = L/4$, where $L{=}L_y{=}L_z{=}L_x/4$ is the width of the computational domain. Subsequently, a forcing function $\boldsymbol{f}$ [see Eq. (2)] was invoked to maintain statically stationary turbulence following the method described in Ref. [42]. As shown earlier [37,38], (i) the rms velocity u_0 was maintained as the initial value, (ii) the normalized dissipation rate $\varepsilon\ell_f/u_0^3$ averaged over the computational domain fluctuated slightly above 3/2 after a short period ($t < \tau_f = \ell_f/u_0$) of rapid transition from the initial artificially synthesized flow to the fully developed turbulence, (iii) the forced turbulence achieved good statistical homogeneity and isotropy over the entire domain, and (iv) the energy spectrum showed a range of the Kolmogorov scaling ($-5/3$) at the Reynolds number $\mathrm{Re}{\equiv}u_0\ell_f/\nu{=}200$ based on the scale ℓ_f (see Fig. 1).

In order to study a fully developed reaction wave, a planar wave $c(\boldsymbol{x},t=0) = c_L(\xi)$ was initially ($t = 0$) released at $x^0 = L_x/2$ such that $\int_{-\infty}^{0} c_L(\xi)d\xi = \int_0^{\infty}[1 - c_L(\xi)]d\xi$ and $\xi = x - x^0$, where $c_L(\xi)$ is the precomputed laminar-wave profile. Subsequently, evolution of this field $c(\boldsymbol{x},t)$ was simulated by solving Eq. (1). To enable periodic propagation of the c field along the x direction, the field is extrapolated outside the axial boundaries of the computational domain at each time step t^n as $c(x',y,z,t^n) = c(x,z,t^n)$, where $x' = x + IL_x$ and I is an arbitrary (positive or negative) integer number. Consequently, Eq. (1) is solved in the interval $x' \in [\zeta(t^n) - \Delta, \zeta(t^n) + \Delta]$, where $\zeta(t^n)$ is the mean coordinate of a reaction wave on the x' axis and $\Delta = 0.45L_x$ in order to avoid numerical artifacts in the vicinity of $x' = \zeta(t^n) \pm 0.5L_x$. In two

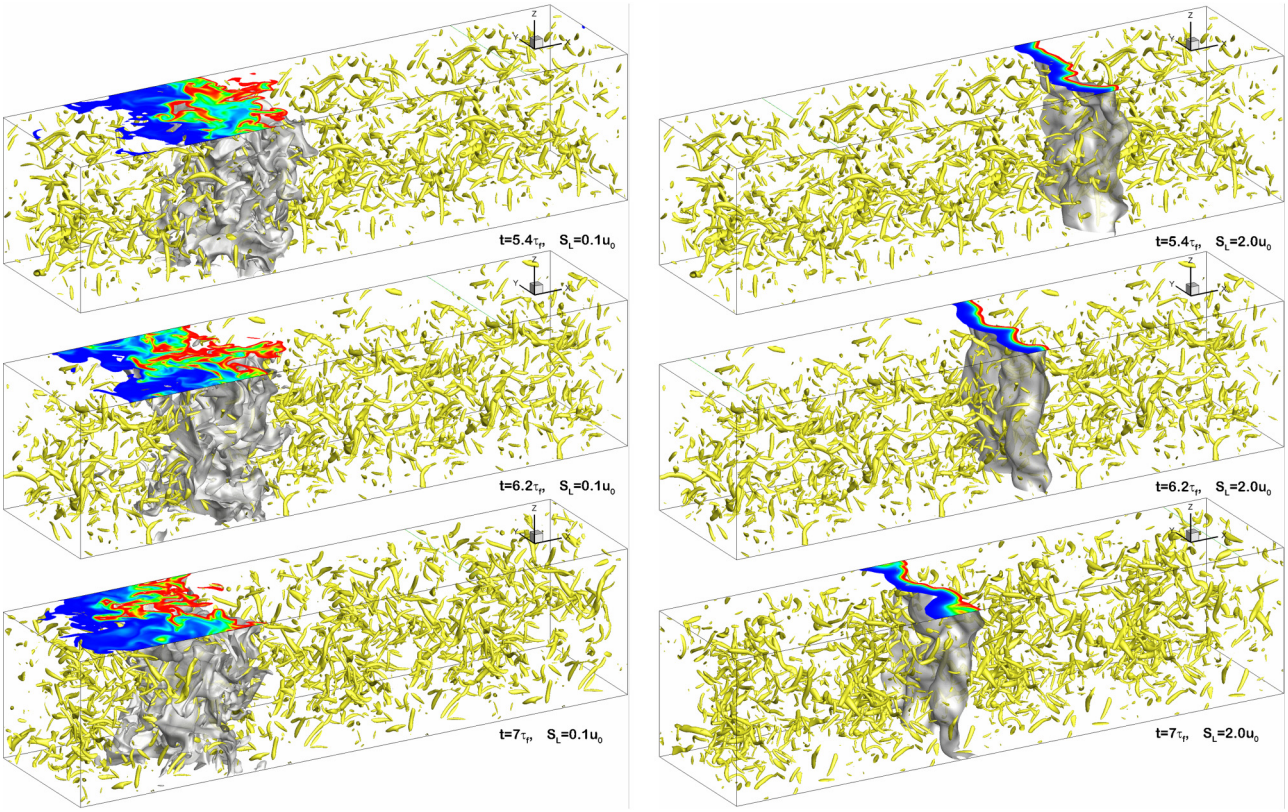

FIG. 2. Instantaneous c field obtained in the DNS at $t/\tau_f = 5.4$ (top row), 6.2 (middle row), and 7 (bottom row) for $\mathrm{Re} = 200$, with $S_L/u_0 = 0.1$ (left column) and 2.0 (right column). Gray isosurfaces are associated with the peak reaction rate, i.e., $c(x,y,z,t) = c^*$, where $W(c^*)$ is the maximum value. Top-sliced planes are colored from blue to red in order to represent an increase in the local c from zero to unity. Yellow vortex tubes visualize turbulence field by showing regions characterized by large values $Q > Q^* = 2u_0^2/\tau_f\nu$ of the Q criterion.

remaining regions, i.e., $x' \in [\zeta(t^n) - 0.5L_x, \zeta(t^n) - \Delta]$ and $x' \in [\zeta(t^n) + \Delta, \zeta(t^n) + 0.5L_x]$, the scalar $c(t^n)$ is set equal to zero (fresh reactants) and unity (products), respectively, because the entire flame brush is always kept within the interval of $x' \in [\zeta(t^n) - \Delta, \zeta(t^n) + \Delta]$ in the present simulations. Finally, the obtained solution $c(x',y,z,t^n)$ is translated back to the x coordinate (for details see [39,40]).

Three turbulent fields were generated by specifying three different initial turbulent Reynolds numbers $\mathrm{Re} = 50$, 100, and 200, which were increased by increasing the domain size L. The increase in L resulted in increasing the longitudinal integral length scale ℓ_{11}, the Taylor length scale $\lambda = \sqrt{15\nu u_0^2/\varepsilon}$, the Taylor scale Reynolds number $\mathrm{Re}_\lambda = u_0\lambda/\nu$, the turbulent time scale $\tau_{11} = \ell_{11}/u_0$, and hence the Damköhler number $\mathrm{Da}_{\mathrm{DNS}} = \tau_{11}/\tau_F$. Henceforth, ε designates the dissipation rate averaged over volume and time at $t > 5\tau_\mathrm{f}$. The simulation parameters are shown in Table I. Because a reaction wave does not affect turbulence in the case of constant density ρ and viscosity ν, the flow statistics were the same in all cases that had different S_L but the same Re. It is worth noting that the longitudinal integral length scale ℓ_{11} reported in Table I and used to evaluate $\mathrm{Da}_{\mathrm{DNS}}$ was averaged over the computational domain and time at $t > 5\tau_\mathrm{f}$ and was lower than its initial value $\ell_\mathrm{f} = L/4$.

When the width L was increased by a factor of 2, the numbers N_x, $N_y = N_x/4$, and $N_z = N_x/4$ were also increased by a factor of 2, i.e., $N_x = 256$, 512, or 1024 at $\mathrm{Re} = 50$, 100, or 200, respectively. Accordingly, in all cases, the Kolmogorov length scale $\eta = (\nu^3/\varepsilon)^{1/4}$ was of the order of the grid cell size Δx (see Table I), thus indicating sufficient grid resolution. The capability of the grids used for resolving well not only the Kolmogorov eddies but also the reaction wave was confirmed in separate (i) one-dimensional simulations of planar laminar reaction waves and (ii) two-dimensional simulations [43] of laminar flames subject to hydrodynamic instability [44]. Moreover, the resolution of the present DNS was validated by running simulations with the grid cell size Δx decreased by a factor of 4 at $\mathrm{Re} = 50$, i.e., by setting N_x equal to 1028.

In the next section we will report the mean quantities $\langle q \rangle$ averaged over a transverse plane and time at $5\tau_\mathrm{f} < t < t_\mathrm{end}$, with t_end being equal to $50\tau_\mathrm{f}$ or even longer. Moreover, we will present correlations between fluctuating quantities $q'(t,\boldsymbol{x}) = q(t,\boldsymbol{x}) - \langle q \rangle(x)$. Furthermore, using the computed axial profiles of $\langle c \rangle$, axial profiles of other mean quantities and correlations will be transformed to dependences of these variables and correlations, respectively, on the mean reaction progress variable $\langle c \rangle$.

IV. RESULTS AND DISCUSSION

Figures 2 shows the evolution of c fields for $\mathrm{Re} = 200$. The background turbulent flow structures are visualized by

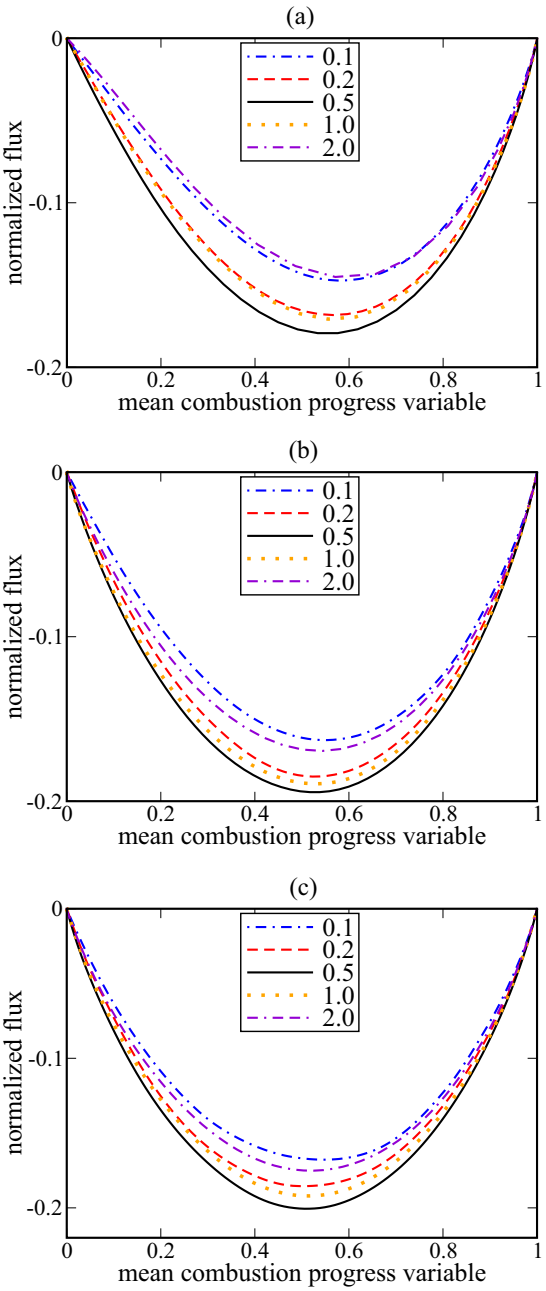

FIG. 3. Dependences of the normalized turbulent scalar flux $\langle u'c'\rangle/u_0$ on the mean reaction progress variable $\langle c\rangle$, computed at different ratios of S_L/u_0 specified in the legend for (a) Re = 50, (b) Re = 100, and (c) Re = 200.

showing regions characterized by large values $Q > Q^* = 2u_0^2/\tau_f\nu$ of the Q criterion. Such a flow structure is typical for homogenous isotropic turbulence. A comparison of these figures shows that a lower normalized laminar-wave speed S_L/u_0 is associated with a more wrinkled surfaces of the reaction zone and a thicker mean turbulent wave brush that propagates at a lower speed.

Figure 3 shows dependences of the normalized turbulent scalar flux $\langle u'c'\rangle/u_0$ on the mean reaction progress variable $\langle c\rangle$, computed for Re = 50 [Fig. 3(a)], Re = 100 [Fig. 3(b)], and Re = 200 [Fig. 3(c)]. In an unburned or burned mixture,

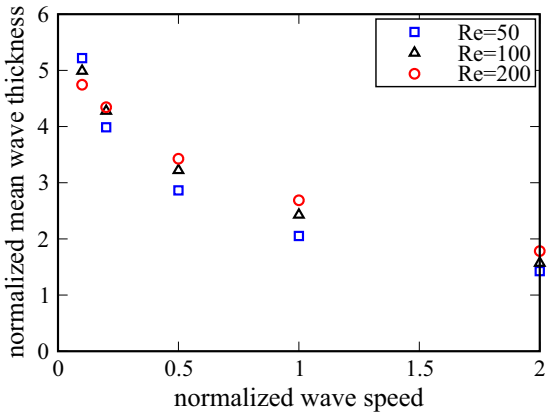

FIG. 4. Dependences of the normalized mean turbulent wave thickness δ_t/ℓ_{11} on the normalized wave speed S_L/u_0 computed at three different turbulent Reynolds numbers Re specified in legend.

the instantaneous progress variable is constant, $c = 0$ or $c = 1$, respectively. This implies that in the two regions turbulent flux $\langle c'\boldsymbol{u}'\rangle = 0$. Inside the mean reaction wave the mean progress variable $\langle c\rangle$ varies between 0 and 1. In this region the gradient $\nabla\langle c\rangle$ does not vanish. Since $\nabla\langle c\rangle$ is positive in this region (in the coordinate framework used in the paper), the turbulent flux $\langle c'\boldsymbol{u}'\rangle = -D_T\nabla\langle c\rangle$ is negative inside the mean reaction wave. The absolute value of the turbulent flux $|\langle c'\boldsymbol{u}'\rangle|$ reaches a maximum at the point where the gradient $\nabla\langle c\rangle$ is maximum. If the probability of deviation of the reaction wave from its mean position is described by the Gaussian distribution, the gradient $\nabla\langle c\rangle$ is maximum at $\langle c\rangle = 0.5$. For instance, in various premixed turbulent flames, $\nabla\langle c\rangle$ does peak at $\langle c\rangle = 0.5$ [see, e.g., Fig. 4.22 and Eqs. (4.34) and (4.35) in [8]]. While the flux magnitude depends on S_L/u_0 and hence on $\mathrm{Da}_{\mathrm{DNS}}$ (see Table I), such variations in the flux magnitude are sufficiently weak and nonmonotonic, with the peak magnitude being obtained at a medium $S_L/u_0 = 0.5$.

In contrast, the mean turbulent wave thickness δ_t defined using the maximum gradient method, i.e.,

$$\delta_t = \frac{1}{\max\{\nabla_x\langle c\rangle\}}, \tag{19}$$

decreases rapidly with the increase of the normalized wave speed S_L/u_0 and hence $\mathrm{Da}_{\mathrm{DNS}}$ (see Fig. 4). This numerical result is fully consistent with the theory, which predicts a decrease in D_T with increasing Damköhler number. Under the DNS conditions, an increase in S_L/u_0 results in increasing Da and therefore decreasing D_T. Consequently, $\delta_t \propto [D_T(\mathrm{Da})\tau_c]^{1/2}$ decreases with increasing S_L/u_0.

Accordingly, the gradient of the mean reaction progress variable is increased by S_L/u_0 (or $\mathrm{Da}_{\mathrm{DNS}}$), whereas turbulent diffusivity evaluated as

$$D_T(\langle c\rangle) = -\frac{\langle u'c'\rangle}{\nabla_x\langle c\rangle} \tag{20}$$

decreases with increasing S_L/u_0 and $\mathrm{Da}_{\mathrm{DNS}}$ (see Fig. 5). The decrease of the turbulent diffusion coefficient D_T with the increase of the Damköhler number observed in DNS agrees well with the developed theory.

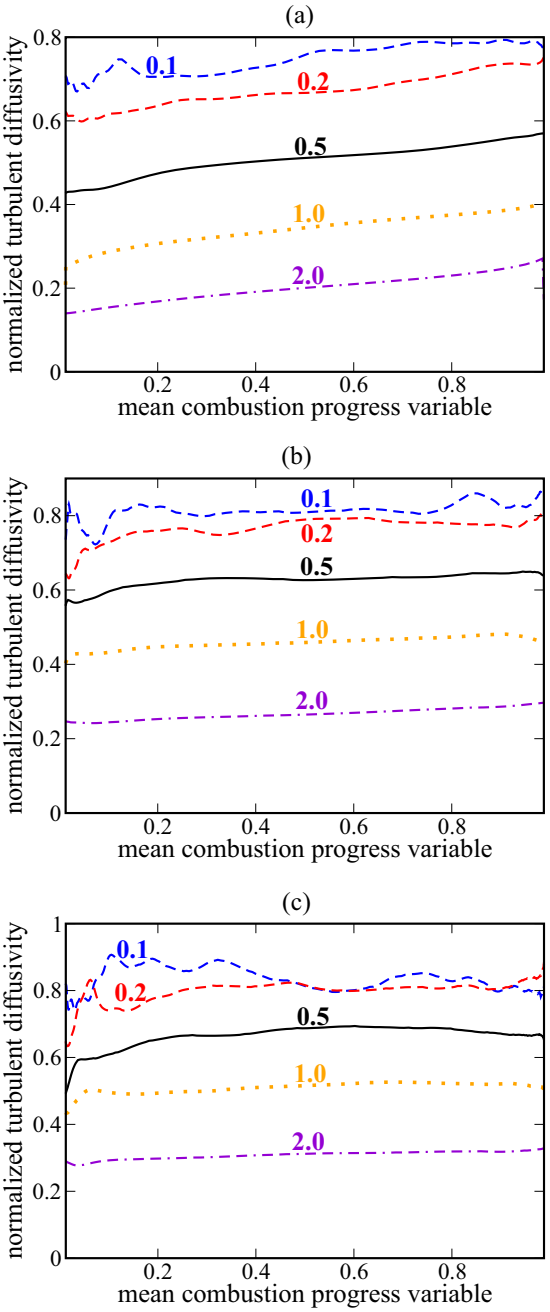

FIG. 5. Dependences of the normalized turbulent scalar diffusivity $D_T/u_0\ell_{11}$ on the mean reaction progress variable $\langle c\rangle$, computed for (a) Re = 50, (b) Re = 100, and (c) Re = 200. Values of S_L/u_0 are specified near the curves.

Moreover, Fig. 5 indicates that D_T evaluated using Eq. (20) depends weakly on $\langle c\rangle$, thus implying that the influence of the reaction on the turbulent diffusion coefficient may be characterized by a single mean turbulent diffusivity defined as

$$\widehat{D_T} = \int_0^1 D_T(\xi)d\xi. \tag{21}$$

To compare values of the mean turbulent diffusion coefficient $\widehat{D_T}$ obtained in the simulations with the theoretical predictions for D_T(Da) we need to take into account that the Damköhler

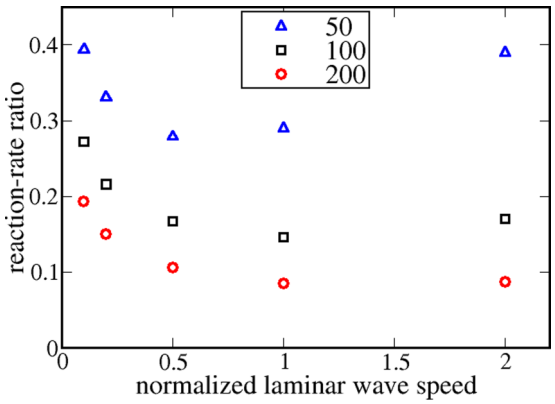

FIG. 6. Reaction-rate ratio $\theta = \max\{\langle W\rangle(\langle c\rangle)\}/\max\{W(c)\}$ vs S_L/u_0. Symbols show DNS data, with the Reynolds numbers Re being specified in the legend.

number $\mathrm{Da_{DNS}}$ used in DNS is different from the Damköhler number Da used in the theory. In the theory, Da involves the time scale τ_c that characterizes the peak mean rate $\langle W\rangle$. In the DNS, due to strong fluctuations in the scalar field $c(t,\boldsymbol{x})$ and especially $W[c(t,\boldsymbol{x})]$, the peak mean rate $\max\{\langle W\rangle(\langle c\rangle)\}$ is much less than the peak local rate $\max\{W[c(t,\boldsymbol{x})]\}$, as is well known in combustion theory [7,8,10–12]. Accordingly, the peak mean reaction rate is characterized by a significantly larger chemical time scale $\langle\tau_c\rangle$ when compared to the time scale τ_F associated with the laminar $W(c)$. A ratio of these two time scales $\theta = \tau_F/\langle\tau_c\rangle = \mathrm{Da}/\mathrm{Da_{DNS}}$ can be estimated as $\theta = \max\{\langle W\rangle(\langle c\rangle)\}/\max\{W(c)\}$. The reaction-rate ratio θ versus S_L/u_0 is shown in Fig. 6 for different values of the Reynolds number Re.

Using the values of θ obtained in the DNS and plotted in Fig. 6, we relate the Damköhler number Da used in the theory with the $\mathrm{Da_{DNS}}$ used in DNS: $\mathrm{Da} = \theta\mathrm{Da_{DNS}}$. In Fig. 7 the mean turbulent diffusion coefficient $\widehat{D_T}$ versus $\mathrm{Da} = \theta\,\mathrm{Da_{DNS}}$ obtained in the simulations (symbols) is compared with the theoretical predictions for D_T given by Eq. (12). Figure 7 demonstrates very good agreement between the results of DNSs and theoretical predictions.

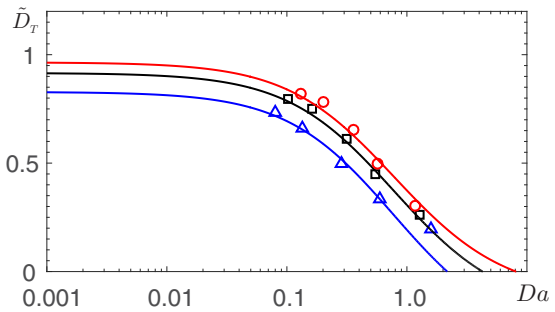

FIG. 7. Theoretical dependence $\tilde{D}_T \equiv D_T/D_0^T$ on Damköhler number Da determined by Eq. (12) for different values of the Reynolds number Re = 50 (blue), 100 (black), and 200 (red) at Pr = 1. The DNS data on $\widehat{D_T}$ normalized using $u_0 l_{11}$ are shown in blue triangles (Re = 50), black squares (Re = 100), and red circles (Re = 200).

V. CONCLUSION

The theory of turbulent diffusion in reacting flows previously developed in [20,21] has been generalized for finite Reynolds numbers and the dependence of turbulent diffusion coefficient on two parameters, the Reynolds number and the Damköhler number, has been obtained. Validation of the generalized theory of the effect of chemical reaction on turbulent diffusion using three-dimensional DNSs of a finite-thickness reaction wave propagation in forced, homogeneous, isotropic, and incompressible turbulence for the first-order chemical reactions has revealed very good quantitative agreement between the theoretical predictions and the DNS results.

ACKNOWLEDGMENTS

This research was supported in part by the Israel Science Foundation governed by the Israeli Academy of Sciences (Grant No. 1210/15) (T.E., N.K., and I.R.), the Research Council of Norway under the FRINATEK (Grant No. 231444) (N.K., M.L., and I.R.), the Swedish Research Council (R.Y.), the Chalmers Combustion Engine Research Center and Chalmers Transport and Energy Areas of Advance (A.N.L.), State Key Laboratory of Explosion Science and Technology, Beijing Institute of Technology (Grant No. KFJJ17-08M) (M.L.). This research was initiated during Nordita Program *Physics of Turbulent Combustion*, Stockholm. The computations were performed on resources provided by the Swedish National Infrastructure for Computing at Beskow-PDC Center.

[1] G. T. Csanady, *Turbulent Diffusion in the Environment* (Reidel, Dordrecht, 1980).
[2] A. K. Blackadar, *Turbulence and Diffusion in the Atmosphere* (Springer, Berlin, 1997).
[3] R. O. Fox, *Computational Models for Turbulent Reacting Flows* (Cambridge University Press, New York, 2003).
[4] N. Peters, *Turbulent Combustion* (Cambridge University Press, Cambridge, New York, 2004).
[5] J. H. Seinfeld and S. N. Pandis, *Atmospheric Chemistry and Physics: From Air Pollution to Climate Change*, 2nd ed. (Wiley, New York, 2006).
[6] L. I. Zaichik, V. M. Alipchenkov, and E. G. Sinaiski, *Particles in Turbulent Flows* (Wiley, New York, 2008).
[7] M. Liberman, *Introduction to Physics and Chemistry of Combustion* (Springer, New York, 2008).
[8] A. N. Lipatnikov, *Fundamentals of Premixed Turbulent Combustion* (CRC, Boca Raton, 2012).
[9] P. A. Libby, Prog. Energy Combust. Sci. **11**, 83 (1985).
[10] K. N. C. Bray, Proc. R. Soc. A **451**, 231 (1995).
[11] A. N. Lipatnikov and J. Chomiak, Prog. Energy Combust. Sci. **36**, 1 (2010).
[12] N. Swaminathan and K. N. C. Bray, *Turbulent Premixed Flames* (Cambridge University Press, Cambridge, 2011).
[13] V. A. Sabelnikov and A. N. Lipatnikov, Annu. Rev. Fluid Mech. **49**, 91 (2017).
[14] V. A. Sabelnikov and A. N. Lipatnikov, Combust. Theory Model. **17**, 1154 (2013).
[15] V. A. Sabelnikov and A. N. Lipatnikov, Phys. Rev. E **90**, 033004 (2014).
[16] V. A. Sabelnikov and A. N. Lipatnikov, Combust. Flame **162**, 2893 (2015).
[17] S. Corrsin, Adv. Geophys. **18A**, 25 (1975).
[18] R. Borghi and D. Dutoya, Proc. Combust. Inst. **17**, 235 (1978).
[19] A. N. Lipatnikov, Proc. Combust. Inst. **33**, 1497 (2011).
[20] T. Elperin, N. Kleeorin, and I. Rogachevskii, Phys. Rev. Lett. **80**, 69 (1998).
[21] T. Elperin, N. Kleeorin, M. A. Liberman, and I. Rogachevskii, Phys. Rev. E **90**, 053001 (2014).
[22] A. Brandenburg, N. E. L. Haugen, and N. Babkovskaia, Phys. Rev. E **83**, 016304 (2011).
[23] A. N. Kolmogorov, I. G. Petrovskii, and N. S. Piskunov, Bull. Moscow State Univ. **1**, No. 6, 1 (1937).
[24] R. A. Fisher, Annals of Eugenics **7**, No. 4, 353 (1937).
[25] S. A. Orszag, J. Fluid Mech. **41**, 363 (1970).
[26] A. S. Monin and A. M. Yaglom, *Statistical Fluid Mechanics* (MIT Press, Cambridge, 1975), Vol. 2.
[27] W. D. McComb, *The Physics of Fluid Turbulence* (Clarendon, Oxford, 1990).
[28] A. Pouquet, U. Frisch, and J. Leorat, J. Fluid Mech. **77**, 321 (1976).
[29] A. Brandenburg and K. Subramanian, Phys. Rep. **417**, 1 (2005).
[30] I. Rogachevskii and N. Kleeorin, Phys. Rev. E **76**, 056307 (2007).
[31] I. Rogachevskii, N. Kleeorin, P. J. Käpylä, and A. Brandenburg, Phys. Rev. E **84**, 056314 (2011).
[32] I. Rogachevskii, N. Kleeorin, A. Brandenburg, and D. Eichler, Astroph. J. **753**, 6 (2012).
[33] P. J. Käpylä, A. Brandenburg, N. Kleeorin, M. J. Mantere, and I. Rogachevskii, Mon. Not. R. Astron. Soc. **422**, 2465 (2012).
[34] A. Brandenburg, O. Gressel, P. J. Käpylä, N. Kleeorin, M. J. Mantere, and I. Rogachevskii, Astroph. J. **762**, 127 (2013).
[35] G. K. Batchelor, *The Theory of Homogeneous Turbulence* (Cambridge University Press, New York, 1953).
[36] R. Yu, J. Yu, and X.-S. Bai, J. Comput. Phys. **231**, 5504 (2012).
[37] R. Yu, A. N. Lipatnikov, and X.-S. Bai, Phys. Fluids **26**, 085104 (2014).
[38] R. Yu, X.-S. Bai, and A. N. Lipatnikov, J. Fluid Mech. **772**, 127 (2015).
[39] R. Yu and A. N. Lipatnikov, Phys. Rev. E **95**, 063101 (2017).
[40] R. Yu and A. N. Lipatnikov, Phys. Fluids **29**, 065116 (2017).
[41] R. Yu and X.-S. Bai, J. Comput. Phys. **256**, 234 (2014).
[42] S. Ghosal, T. S. Lund, P. Moin, and K. Akselvoll, J. Fluid Mech. **286**, 229 (1995).
[43] R. Yu, X.-S. Bai, and V. Bychkov, Phys. Rev. E **92**, 063028 (2015).
[44] L. D. Landau and E. M. Lifshitz, *Fluid Mechanics*, 2nd ed. (Elsevier, Oxford, 2009).